

Localized surface plasmon assisted microfluidic mixing

Xiaoyu Miao,^{a)} Benjamin K. Wilson, and Lih Y. Lin

Electrical Engineering Department, University of Washington, Seattle, Washington 98195, USA

(Received 11 January 2008; accepted 29 February 2008; published online 28 March 2008)

We present an optical microfluidic mixing approach via thermally induced convective flow sustained by localized surface plasmon (LSP) energy. The phonon energy associated with the nonradiative damping of LSP from a Au nanoparticle (NP) array under optical excitation creates a thermal gradient which initiates a convective fluidic flow. Experimental evidence and modeling results both show that LSP from the Au NPs is crucial in establishing a temperature gradient with sufficient magnitude to induce the convective flow with low input optical intensity. © 2008 American Institute of Physics. [DOI: 10.1063/1.2901192]

Microfluidic devices that perform various chip-based chemical and biological analyses have received significant attention in the past few years. The enthusiasm is triggered by several advantages of the devices: high throughput, short analysis time, reduced sample volumes, and the possibility for *in situ* operation.¹ Microfluidic devices attempt to incorporate the necessary components and functionalities of a typical laboratory on the surface of a substrate to achieve a “laboratory on a chip.” Many chemical and biological analysis methods such as immunoassay, cell-molecule interaction, and DNA hybridization require localized, rapid mixing. In miniaturized devices, the mixing processes for fluids with low Reynolds numbers can take a considerably long time. This is particularly true when the solution contains macromolecules with a low molecular diffusion coefficient.² Various approaches have been developed to facilitate microfluidic mixing. These approaches can be generally categorized into passive and active mixings. Passive mixing is typically accomplished by driving fluids through channels with complex and fixed geometries. This often involves complex design and fabrication of microchannels.³ Active mixing uses an external energy source to destabilize the flow fields. The advantage of active mixing is that it can be activated on demand. Several active mixing methods have been demonstrated, including those using ultrasound,⁴ magnetic actuation,⁵ and electro-osmotic flow.⁶ Compared to these conventional active mixing approaches, using light as the input energy source for microfluidic mixing has many unique advantages. This is because optical excitation is precise, reconfigurable, and easy to integrate with various laboratory-on-a-chip devices. Recently, laser induced mixing in microfluidic channels has been realized by using a highly focused nanosecond pulsed laser to form plasma and cavitation bubbles in the fluids.⁷ The bubble expansion and subsequent collapse within the microfluidic channels disrupt the laminar flow and produce a localized region of mixed fluid. One drawback of this approach is that it relies on plasma formation which requires a pulsed laser with extremely high intensity. The average intensity threshold is reported to be $7.6 \times 10^{10} \text{ W cm}^{-2}$ for a 6 ns neodymium doped yttrium aluminum garnet (Nd:YAG) pulsed laser.⁸ Such intense light can cause some undesirable side effects, such as photodamage in biological applications.⁹ In this paper, we propose and demonstrate an active mixing approach employing light-induced

localized surface plasmons (LSPs). Experimental results show that this approach requires very low optical intensity to achieve the mixing operation in a microfluidic environment.

LSPs are the collective electron oscillations confined in metal nanoparticles (NPs) excited by light. The nonradiative decay of plasmon energy is associated with the dissipation of these oscillations. Effectively, the oscillation of the electrons is a current which is damped by the resistance of the metal. Ultimately, the energy dissipated through the nonradiative process is transferred into heat. Such photothermal effect has already been used in controlled modulation of drug delivery,¹⁰ chemical vapor deposition,¹¹ and guiding of liquid flow.¹² Here, we demonstrate active microfluidic mixing through the photothermal effect of LSP from a Au NP array. The nonradiative decay of the plasmon energy creates a localized heat source on the surface of the NP array. When the temperature gradient at the surface exceeds a threshold, a convective fluidic flow will be formed to dissipate the energy in the liquid layer above the Au NP array. The convective flow drives the liquid out from the region around the heat source and pulls in cooler liquid, which can be used to mix the liquid. Thanks to the enhanced absorption efficiency of Au NPs, the induced convective flow can be very strong with low input optical intensity. In other words, the LSP induced microfluidic mixing can achieve high optical-to-thermal energy conversion efficiency.

In the context of our present work, the experimental configuration is depicted in Fig. 1. A microfluidic chamber is formed by sealing two glass coverslips with polymethylsiloxane (PDMS). The liquid is introduced to the microfluidic chamber through a pipette. The thickness of the liquid layer is determined by the thickness of the PDMS layer and estimated to be about $10 \mu\text{m}$. The bottom glass coverslip is covered with a random Au NP array. A HeNe laser is directed

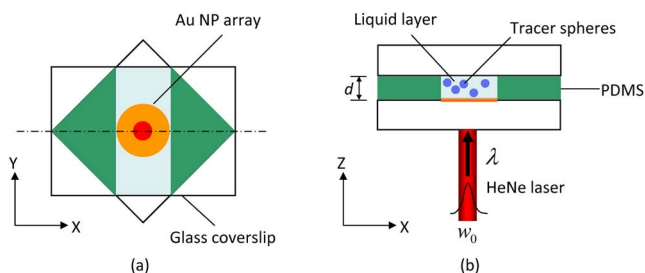


FIG. 1. (Color online) (a) Top view and (b) side view of the schematic experimental configuration.

^{a)}Electronic mail: xiaoyu@ee.washington.edu.

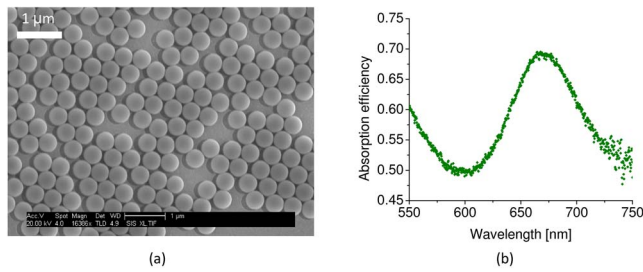


FIG. 2. (Color online) (a) SEM micrograph of the cap-shaped Au NP array. (b) Absorption spectrum of the cap-shaped Au NP array with the peak located at ~ 670 nm.

in the upward direction and focused onto the Au NP array by a biconvex lens. A neutral density filter is used to adjust the input laser power. Once the intensity of the input laser reaches a threshold, a convective flow is formed in the liquid layer. The induced fluidic flow is visualized by dyed polystyrene spheres (PolySciences, Inc.). The motion of the tracer spheres is monitored by a fluorescence microscope (Zeiss Axio Imager) under dark field configuration.

To fabricate the Au NP array on the glass coverslip, a chemical self-assembly approach is adopted using the surface-adsorbed latex spheres (Polysciences, Inc.) with a mean diameter of 454 nm. The latex sphere monolayer is self-assembled by exposing a Au-coated glass coverslip to a mixture of 1-ethyl-3-(3-dimethylaminopropyl) carbodiimide hydrochloride (EDC), latex sphere suspension and de-ionized water. The adsorption process is allowed to last for about 1 h and the nonabsorbed spheres are rinsed off with water. Subsequently, a Au layer (20 nm) is evaporated on the self-assembled latex sphere template and forms a cap-shaped Au NP array. Scanning electron microscopy (SEM) is used to characterize the morphology of the sample. The image in Fig. 2(a) shows a monodispersed distribution of Au NPs with a good coverage. The scattering and extinction spectra are both measured using an UV/visible spectrometer and normalized to the spectrum of incident light. The absorption efficiency spectrum is then obtained by subtracting the normalized scattering spectrum from the normalized extinction spectrum. This efficiency represents the percentage of incident light absorbed by the Au NP array. Figure 2(b), showing the absorption efficiency spectrum, indicates a peak at ~ 670 nm.

Figures 3(a)–3(d) show a sequence of top-view snapshots which demonstrate the operation of microfluidic mixing. The convective flow of the liquid is induced when the HeNe laser is turned on close to the liquid-air interface (shown as the bright green line in Fig. 3). The minimum optical intensity measured at the surface of the Au NP array to induce such convective flow is found to be $6.4 \times 10^3 \text{ W cm}^{-2}$, which is about seven orders of magnitude less than the optical intensity required for plasma formation.⁸ The rapid motion of tracer spheres shown in Fig. 3(c) indicates a strong convective flow, and therefore efficient localized mixing. The velocity profile of the liquid flow can be visualized by the moving trajectory of tracer spheres, which flows out of the central hot region and returns back to the center through the bulk region, forming multiple vortices. The mixing process can be precisely modulated by switching the laser light on and off. To verify the role of LSP in the mixing process, we conducted a control experiment under

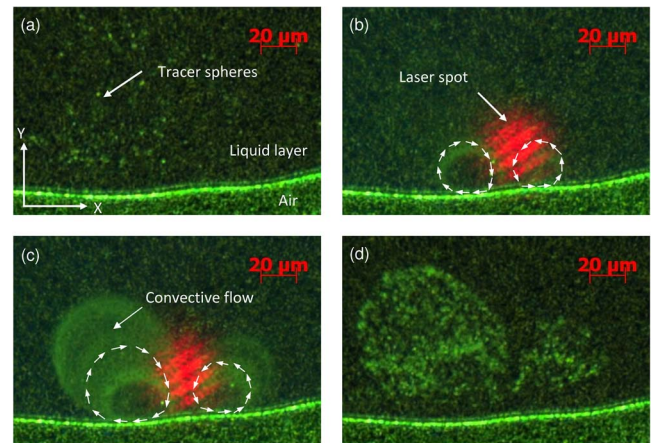


FIG. 3. (Color online) Demonstration of the LSP driven microfluidic mixing visualized by the dyed polystyrene tracer spheres with a diameter of $1 \mu\text{m}$. The snapshots are top views of the sample. (a) When the laser is off, the motions of the tracer spheres are only induced by diffusion, which are very slow. (b) When the laser is turned on, the incident light beam through LSP forms a localized heat source at the location of the red spot. The convective flow of the fluid starts without noticeable delay. (c) The convective flow of the fluid becomes stronger and reaches a steady state under continuous light radiation. The velocity fields of fluidic flow exist at both the right and left sides of the light spot. (d) The tracer spheres start to diffuse away after the laser is turned off.

the same configuration but without the Au NP array. There is no fluid motion observed even with a higher laser intensity of $8.0 \times 10^3 \text{ W cm}^{-2}$, which corresponds to the maximum output from our laser. This indicates that the LSP from Au NPs is crucial in realizing the mixing operation.

To explain the different behaviors of fluids with and without the existence of Au NPs, the heat fluxes in both situations are analyzed as follows. In the absence of Au NPs, the heat generation in the system is purely attributed to the absorption of the optical energy by the liquid layer. In this situation, the induced heat flux in the liquid layer can be calculated as $J_1 = (1 - e^{-\alpha d}) I_0$, where α is the absorption coefficient of the liquid, d is the thickness of the liquid layer, and I_0 is the optical intensity of the incident laser beam. By substituting the parameter values shown in Table I, the conversion ratio from optical-to-thermal energy is calculated to be about 3×10^{-7} , which suggests that light absorption by the liquid layer is not an efficient optical-to-thermal energy conversion process. When the Au NPs are present, there are two basic mechanisms contributing to the heat generation: (i) absorption of incident light and scattered light from the Au NP array by the liquid layer and (ii) nonradiative decay of LSP energy from the excited Au NP array. The heat generation through the first mechanism is almost negligible compared to the second one. Therefore, the heat flux generated in the system can be approximated as the energy intensity absorbed by the Au NP array, which can be calculated as $J_2 = Q_{\text{abs}} I_0$,

TABLE I. Physical parameters.

Symbol	Parameter	Value
d	Thickness of liquid layer	$10 \mu\text{m}$
α	Absorption coefficient of liquid	0.3 m^{-1}
η	Density of liquid	1000 kg m^{-3}
ρ	Thermal conductivity of liquid	$0.58 \text{ W m}^{-1} \text{ K}^{-1}$
C	Thermal capacity of liquid	$4185.5 \text{ J kg}^{-1} \text{ K}^{-1}$
k	Thermal conductivity of liquid	$0.58 \text{ W m}^{-1} \text{ K}^{-1}$

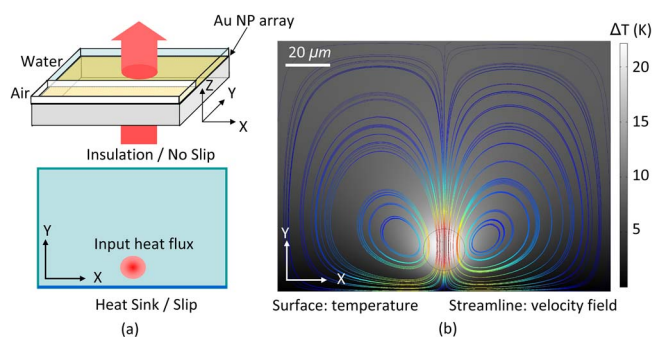


FIG. 4. (Color online) (a) Configuration for the FEMLAB modeling. (b) Modeling results showing temperature distribution and flow streamlines at a planar cross section of the liquid layer.

where Q_{abs} is the absorption efficiency of the Au NP array. This value has been experimentally obtained [Fig. 2(b)] and is about 0.54 at the wavelength of the HeNe laser (633 nm). The above results suggest that the optical-to-thermal energy conversion ratio with the existence of LSP from Au NPs is about six orders of magnitude higher than that without the Au NPs. The above analysis provides support to the experimental observations that the LSPs from Au NPs are critical to inducing the convective flow under our experimental conditions.

In order to investigate the temperature increase of the system and velocity field of the fluidic flow, further numerical simulation is conducted using FEMLAB. The time independent Navier–Stokes equation, $\rho(\vec{v} \cdot \nabla)\vec{v} + \nabla \cdot p - \eta \nabla^2 \vec{v} = \vec{F}$, and the continuity equation for incompressible Newtonian flow, $\nabla \cdot \vec{v} = 0$, are solved numerically together with the thermal transfer equation $\nabla \cdot (-k \nabla T + \rho C T \vec{v}) = Q$, where \vec{v} is the velocity vector, p is the pressure, \vec{F} is the external force, Q is the input heat flux, and η , ρ , C , and k denote the viscosity, density, heat capacity, and thermal conductivity of the fluid, respectively. Figure 4(a) shows the schematic layout of the model and the boundary settings. The input heat source is assumed to exist close to the liquid-air interface. The profile of the heat flux is assumed to be Gaussian and centered at the source. The external force term is set proportional to the temperature gradient. The liquid-air interface is defined as

having slip and assumed to be a heat sink. No-slip conditions are applied for the other three boundaries of the liquid layer and they are assumed to be adiabatic. The complete set of differential equations is discretized in a finite element methodology and solved iteratively until convergence is obtained. The numerical results are presented in Fig. 4(b), which shows that the highest temperature increase in the liquid layer is about 22 K, and that the fluidic flow is formed at both sides of the heat source, similar to what we observed in the experiment. This numerical study confirms the mixing behavior experimentally observed and justifies the use of LSP as an effective energy conversion mechanism for such application.

In summary, we have demonstrated an efficient all-optical microfluidic mixing approach by utilizing the LSP from a Au NP array. Optimized design of the Au NP array to increase the absorption efficiency can further enhance the performance. The presented approach may find broad applications in the emerging area of optofluidics.

This work is supported by the National Science Foundation (DBI 0454324) and the National Institute of Health (R21 EB005183).

- ¹D. J. Beebe, G. A. Mensing, and G. M. Walker, *Annu. Rev. Biomed. Eng.* **4**, 261 (2002).
- ²C. J. Campbell and B. A. Gryzbowski, *Philos. Trans. R. Soc. London, Ser. A* **362**, 1069 (2004).
- ³A. D. Stroock, S. K. W. Dertinger, A. Ajdari, I. Mezic, H. A. Stone, and G. M. Whitesides, *Science* **295**, 647 (2002).
- ⁴G. G. Yaralioglu, I. O. Wygant, T. C. Marentis, and B. T. Khruai-Yahub, *Anal. Chem.* **76**, 3694 (2004).
- ⁵L. Lu, K. S. Ryn, and C. Liu, *J. Microelectromech. Syst.* **11**, 462 (2002).
- ⁶M. H. Oddy, J. G. Santiago, and J. C. Mikkelsen, *Anal. Chem.* **73**, 5822 (2001).
- ⁷A. N. Hellman, K. R. Rau, H. H. Yoon, S. Bae, J. F. Palmer, K. S. Philips, N. L. Allbritton, and V. Venugopalan, *Anal. Chem.* **29**, 4484 (2007).
- ⁸A. Vogel, K. Nahen, D. Theisen, and J. Noack, *IEEE J. Sel. Top. Quantum Electron.* **2**, 847 (2007).
- ⁹K. C. Neumann, E. H. Chadd, G. F. Liou, K. Bergman, and S. M. Block, *Biophys. J.* **70**, 1529 (1999).
- ¹⁰S. R. Sershen, S. L. Westcott, N. J. Halas, and J. L. West, *J. Biomed. Mater. Res.* **51**, 293 (2000).
- ¹¹D. A. Boyd, L. Greengard, M. Brongersma, M. Y. El-Naggar, and D. G. Goodwin, *Nano Lett.* **6**, 2592 (2006).
- ¹²G. L. Liu, J. Kim, Y. Lu, and L. P. Lee, *Nat. Mater.* **5**, 27 (2005).